Electronic Supplementary Material (ESI) for Materials Advances.

Supporting Information

Cu atomic clusters on N-doped porous carbon with tunable chemical state for highly-selective electroreduction of CO_2

Jin Gao,[a] Hui Wang,[a] Kun Feng,[a] Chensheng Xiang,[b] Huibo Wang,[a] Huihui Qi,[a] Yang Liu,*[a] He Tian,*[b] Jun Zhong,*[a] Zhenhui Kang*[a]

[a]Institute of Functional Nano and Soft Materials Laboratory (FUNSOM), Jiangsu Key Laboratory for Carbon-Based Functional Materials & Devices, Soochow University, 199 Ren'ai Road, Suzhou 215123, PR China.

[b]Center of Electron Microscopy, State Key Laboratory of Silicon Materials, School of Materials Science and Engineering, Zhejiang University, Hangzhou 310027, Zhejiang, China.

*Correspondence to: yangl@suda.edu.cn (Y Liu), hetian@zju.edu.cn (H Tian), jzhong@suda.edu.cn (J Zhong), zhkang@suda.edu.cn (ZH Kang)

1. Experimental Section

1.1 Preparation of ZnO@ZIF-8.

$Zn(CH_3COO)_2 \cdot 2H_2O$ (34.9 mmol) was dissolved in 700 mL ethanol and then magnetically stirred for 30 min at 75 ºC until the zinc solution turn to clarifying. Then 30 mL of KOH ethanol solution (2 mol L^{-1}) was added into the above solution under magnetically stirred at 75ºC for 10 min to obtain ZnO QDs solution. $ZnCl_2 \cdot 2H_2O$ (9.9 mmol) was dissolved in 200 mL ethanol, meanwhile 2-methylimidazole (2-MeIM) (36.7 mmol) was dissolved in 100 mL ethanol. Then 200 mL $ZnCl_2 \cdot 2H_2O$ ethanol solution was added into the above ZnO QDs solution with magnetically stirred at the room temperature, and then 100 mL of 2-MeIM ethanol solution was poured into the above solution as well. Finally, the mixture solution was magnetically stirred for 24 h. The product was collected by centrifuge (8000 rpm, 2 min) and then divided into 6 equal portions and dried in vacuum at 50 ºC for 6 h.

1.2 Preparation of mesoporous N-doped carbon material (NPC).

1/6 collected ZnO@ZIF-8 product was placed in the hot center of a horizontal tube furnace in a porcelain boat. The sample was heated at 900 ℃ for 2 h in N_2 atmosphere. After that, the black powder of N-doped mesoporous carbon material was obtained.

1.3 Preparation of copper nanoparticles supported on N-doped porous carbon material (Cu NPs/NPC).

1/6 collected ZnO@ZIF-8 product was put into a 100 mL beaker, then 40 mL $CuCl_2$ solution (6 mmol) was added and stirred for 40 min at room temperature in order to make the salt solution completely absorbed. Then the sample was centrifuged and dried in vacuum at 50°C for 6 h. The sample was placed in a tube furnace and heated to 900 °C for 2h in a stream of N_2 to yield Cu NPs/NPC. The Cu content was measured to be 2.3 wt% based on the ICP analysis.

1.4 Preparation of bulk spinous copper supported on N-doped porous carbon material (Bulk Cu/NPC).

1/6 collected ZnO@ZIF-8 product was put into a 100 mL beaker, then 40 mL $CuCl_2$ solution (10 mmol) was added and stirred for 40 min at room temperature in order to make the salt solution completely absorbed. Then the sample was centrifuged and dried in vacuum at 50°C for 6 h. The sample was placed in a tube furnace and heated to 900 °C for 2h in a stream of N_2 to yield Bulk Cu/NPC. The Cu content was measured to be 4.8 wt% based on the ICP analysis.

1.5 Gas adsorption measurements.

All the gas adsorptions were examined on a Micromeritics ASAP 2050 instrument. For N_2, the catalysts were degassed at 120 °C for 2 h before analysis. Isotherms were analyzed using ASIQwin software. The surface areas of the samples were determined from nitrogen sorption isotherms at 77 K. Pore-size distributions of the samples were calculated from the nitrogen sorption isotherms using nonlocal density functional theory (NLDFT). CO_2 adsorption was determined by plotting the adsorption isotherm of CO_2 at 25 °C. The samples were degassed for two cycles before analysis.

1.6 Calculation of Faradaic efficiencies.

The Faradaic efficiencies of CO and H_2 were calculated according to the following equations:

For CO,

$$FE_{CO} = \frac{z \times n_{CO} \times F}{Q} \times 100\% \quad (1)$$

For H_2,

$$FE_{H_2} = \frac{z \times n_{H_2} \times F}{Q} \times 100\% \quad (2)$$

Where: z is the number of electrons exchanged, for example, z=2 for reduction of CO_2 to CO. F is the Faraday constant (F=96485 C/mol), n_{CO} is the number of moles for the produced CO, and n_{H_2} for the produced H_2, which are measured by GC. Q is the total charge passed.

1.7 Electrochemical measurements.

All electrochemical tests were carried out at room temperature using a H-type three-electrode cell. Three electrodes were the reference electrode (saturated calomel electrode; SCE), counter electrode (platinum wire) and working electrode (catalyst-modified carbon fiber paper electrode (1 cm*2 cm)), respectively. The catalyst ink concentration was 6 mg mL^{-1} in which the solvent was Nafion ionomer solution (0.5 wt %). Generally, 400 μL of the catalyst ink (200 μL in each side) was loaded onto the carbon fiber paper electrode.

The catalyst performance was measured in 0.5 M $KHCO_3$ electrolyte under CO_2 and N_2 atmospheres by linear sweep voltammetry (LSV) for comparison, respectively. In addition, the constant-potential electrolysis for the products analysis was measured in a gas-tight H-type cell. Nafion®212 proton exchange membrane was used to separate two components of the cell. Each of the two compartments contains 30 mL of electrolyte with 20 mL headspace above the electrolyte (each part volume is 50 mL).

All potentials were converted to the reversible hydrogen electrode (RHE) scale through the Nernst equation ($E_{RHE}= E_{SCE}+ 0.0591\times pH+0.2412$ V, at 25 °C).

Gas chromatography (GC, PERSEE G5) equipped with two detectors (thermal conductivity detector (TCD) and flame ionization detector (FID)) was used to detect the gaseous products. NMR (Bruker AVANCE III 600) spectroscopy was applied for the identification of the liquid products. The detected solution consists of 0.5 mL electrolyte, 0.1 mL D_2O solvent and 0.05 μL dimethyl sulfoxide (DMSO, Sigma, 99.99%).

2. Supplementary figures.

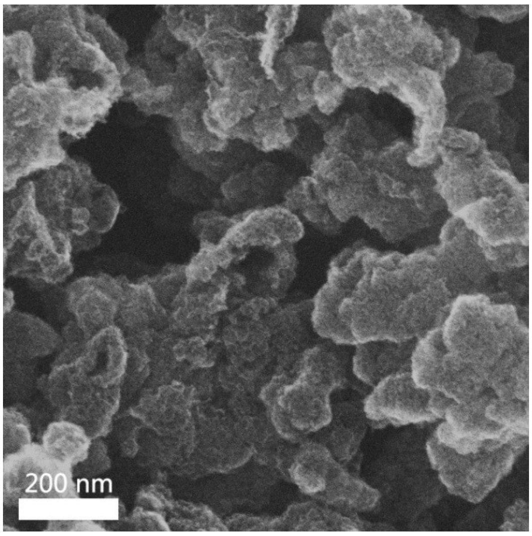

Figure S1. SEM image of Cu ACs/NPC.

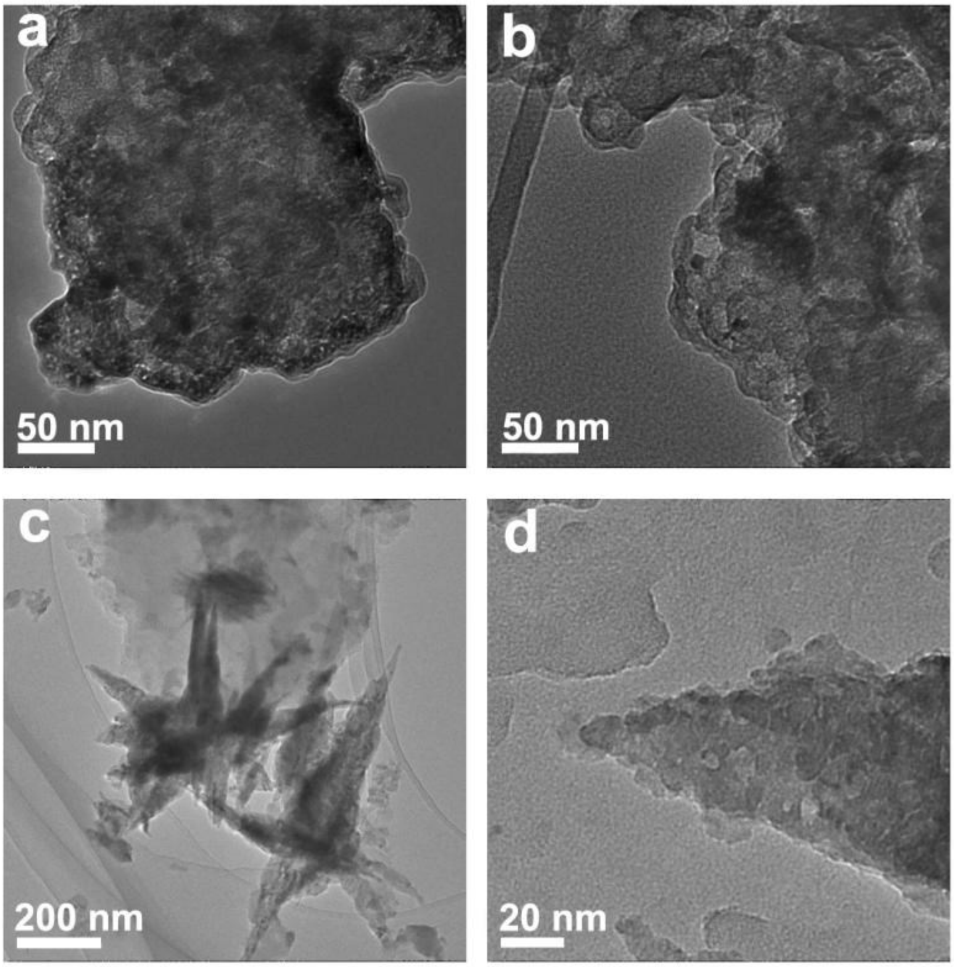

Figure S2. HRTEM images of (a, b) Cu nanoparticles dispersed on N-doped porous carbon matrix (Cu NPs/NPC) and (c, d) bulk spinous Cu dispersed on N-doped porous carbon matrix (Bulk Cu/NPC).

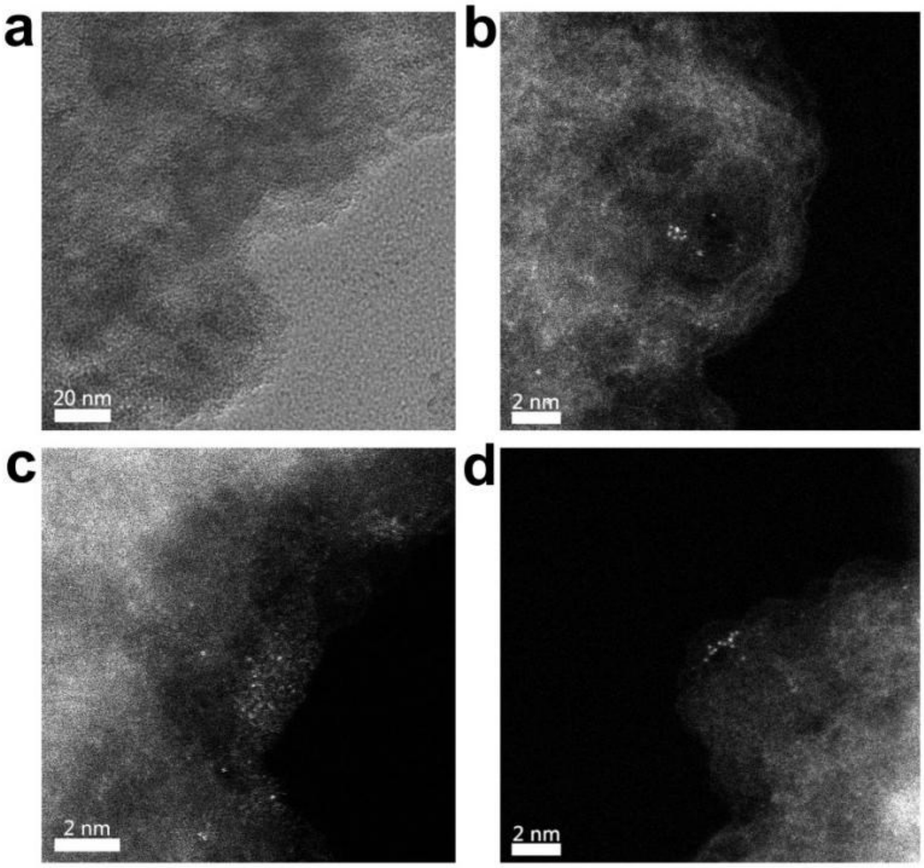

Figure S3. HAADF-STEM images of Cu ACs/NPC in different regions.

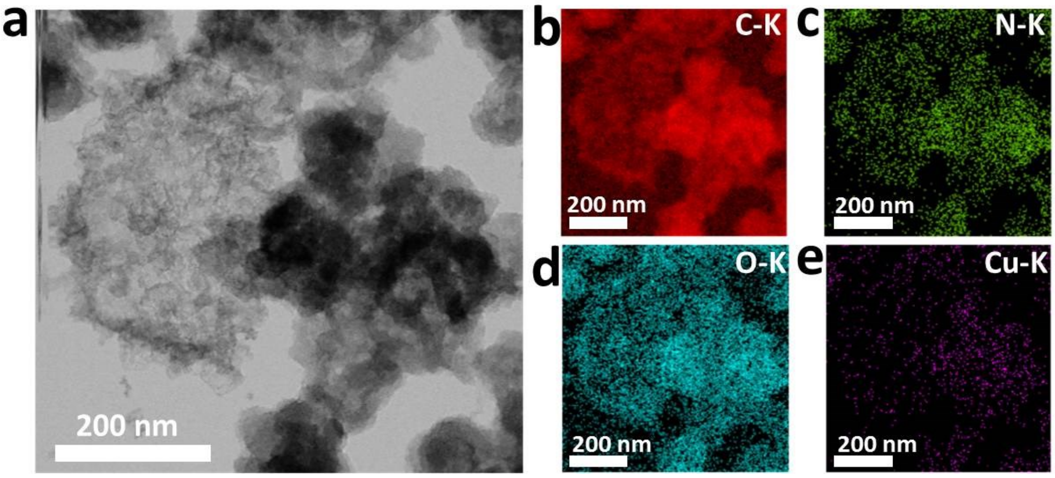

Figure S4. (a) STEM image of Cu ACs/NPC. EDX mapping profiles of different elements in sample a: (b) C, (c) N, (d) O, and (e) Cu, respectively.

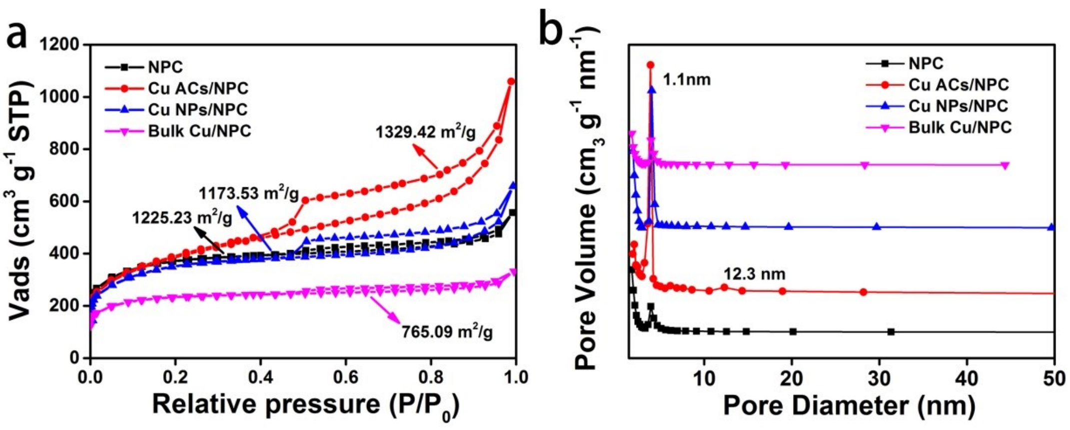

Figure S5. (a) N_2 adsorption-desorption isotherms and (b) pore size distribution of NPC (black line), Cu ACs/NPC (red line), Cu NPs/NPC (blue line) and Bulk Cu/NPC (pink line).

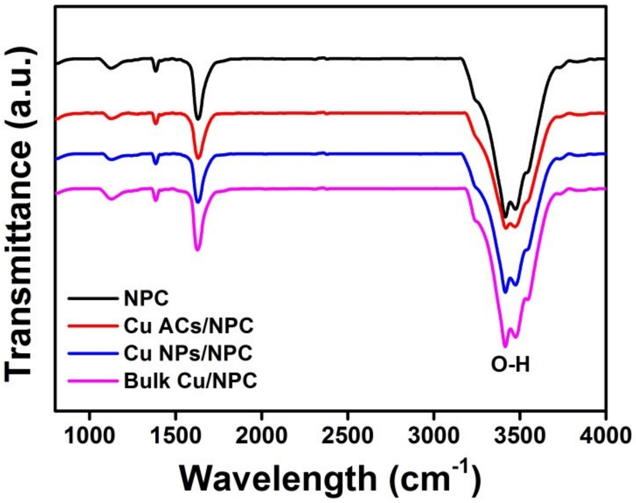

Figure S6. FT-IR spectra of NPC (black line), Cu ACs/NPC (red line), Cu NPs/NPC (blue line) and Bulk Cu/NPC (pink line).

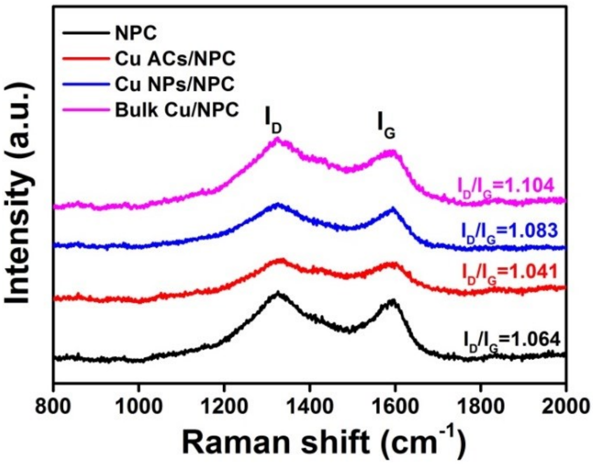

Figure S7. Raman spectra of NPC (black line), Cu ACs/NPC (red line), Cu NPs/NPC (blue line) and Bulk Cu/NPC (pink line).

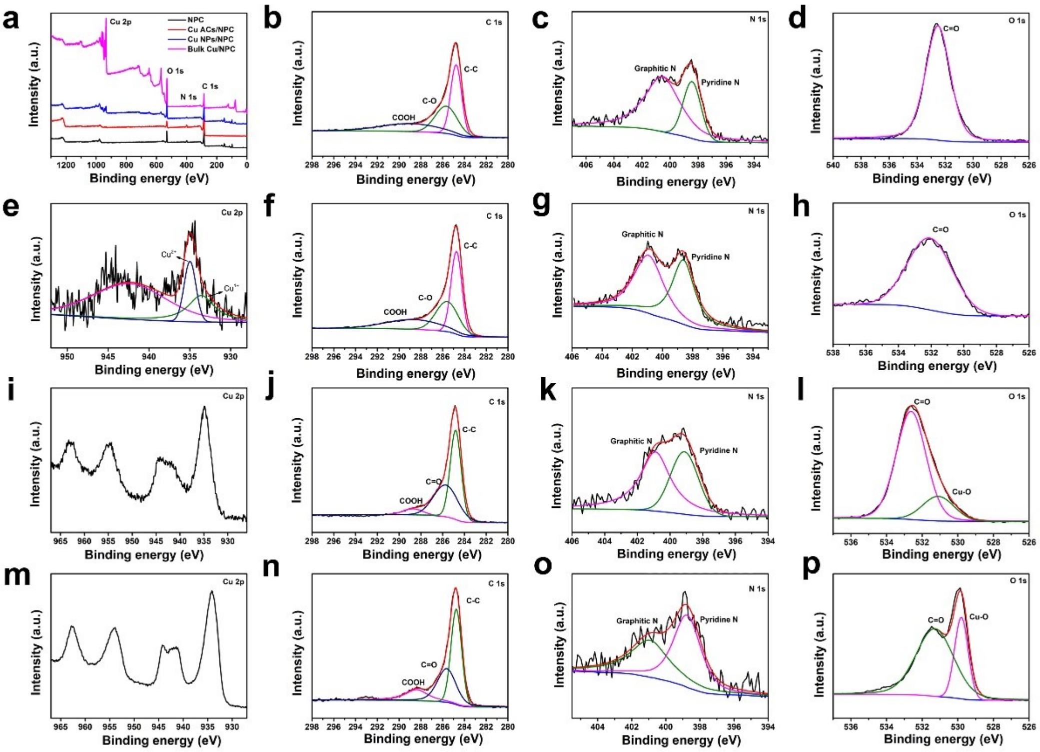

Figure S8. (a) XPS survey spectra of NPC, Cu ACs/NPC, Cu NPs/NPC and Bulk Cu/NPC. (b, c, d) C1s, N 1s and O 1s high-resolution spectra of NPC. (e, f, g, h) Cu 2p, C1s, N 1s and O 1s high-resolution spectra of Cu ACs/NPC. (i, j, k, l) Cu 2p, C1s, N 1s and O 1s high-resolution spectra of Cu NPs/NPC. (m, n, o, p) Cu 2p, C1s, N 1s and O 1s high-resolution spectra of Bulk Cu/NPC.

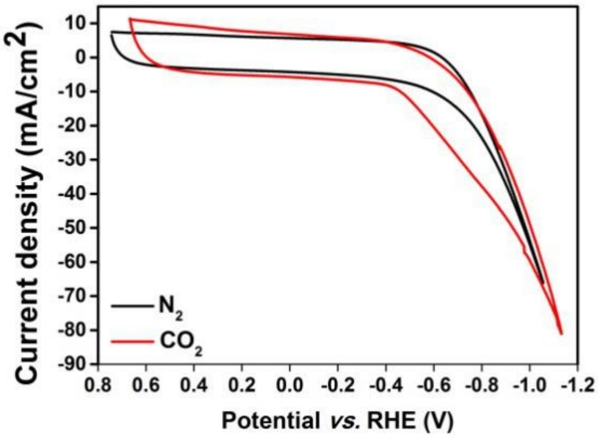

Figure S9. Cyclic voltammograms of Cu ACs/NPC on GC electrode in N_2 and CO_2 saturated 0.5 M $KHCO_3$ at a scan rate of 50 mV s^{-1}.

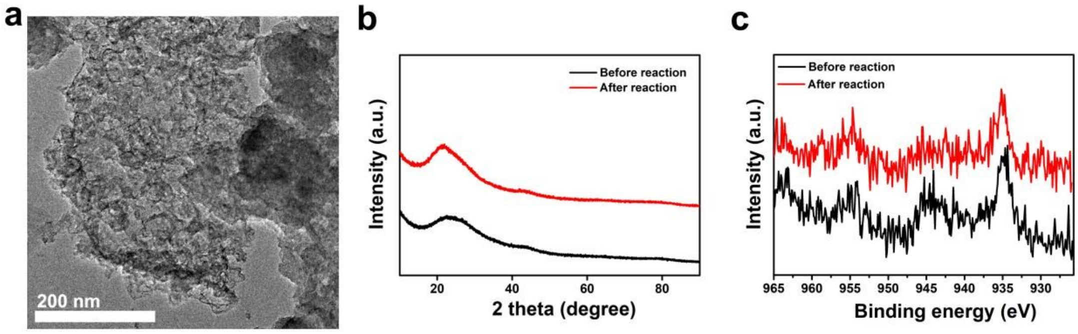

Figure S10. (a) TEM image of Cu ACs/NPC after 24-h electrolysis. (b) XRD patterns and (c) Cu 2p XPS spectra of Cu ACs/NPC before and after 24-h electrolysis.

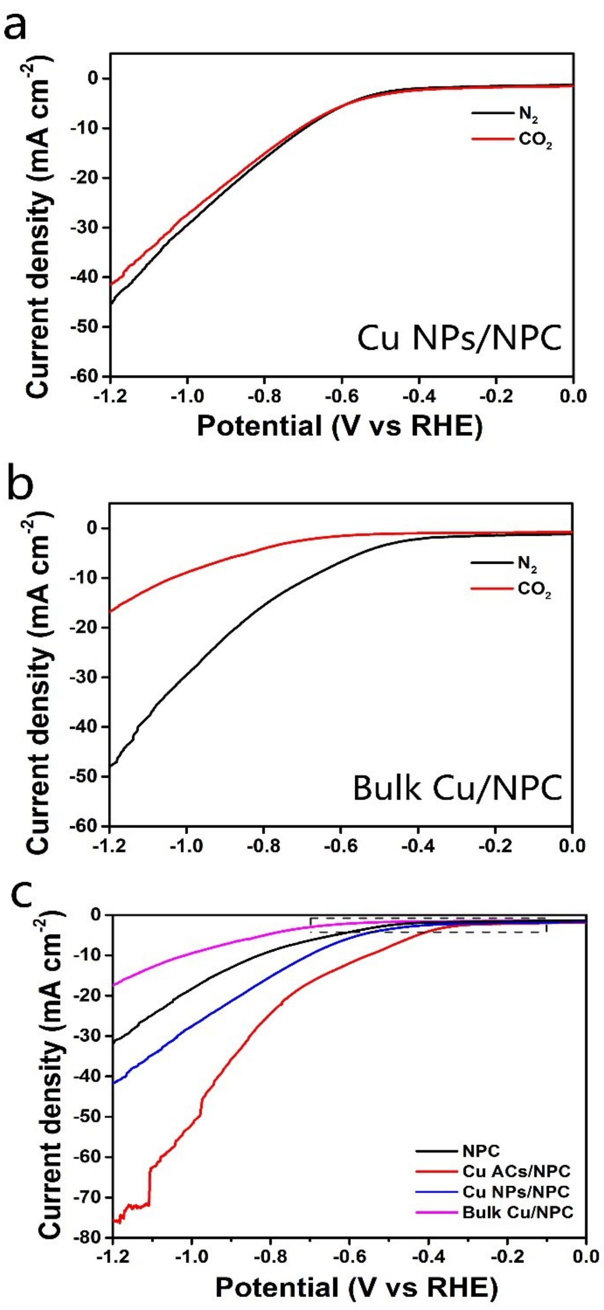

Figure S11. LSV curves for (a) Cu NPs/NPC and (b) Bulk Cu/NPC measured in N_2-saturated (black trace) and CO_2-saturated (red trace) 0.5 M $KHCO_3$ electrolytes with a scan rate of 20 mV s^{-1}. (c) LSV curves for NPC, Cu ACs/NPC, Cu NPs/NPC and Bulk Cu/NPC in CO_2-saturated 0.5 M $KHCO_3$ electrolyte.

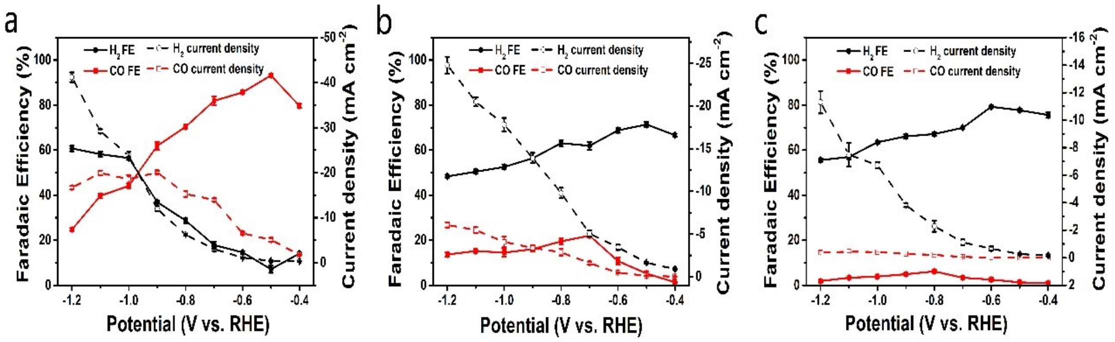

Figure S12. CO and H_2 Faradaic efficiencies and partial current densities for (a) Cu ACs/NPC, (b) Cu NPs/NPC, and (c) Bulk Cu/NPC.

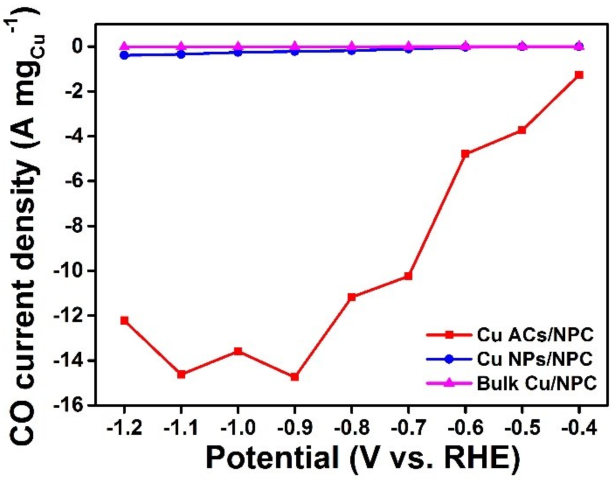

Figure S13. Mass specific CO partial current densities for Cu ACs/NPC (red line), Cu NPs/NPC (blue line) and Bulk Cu/NPC (pink line).

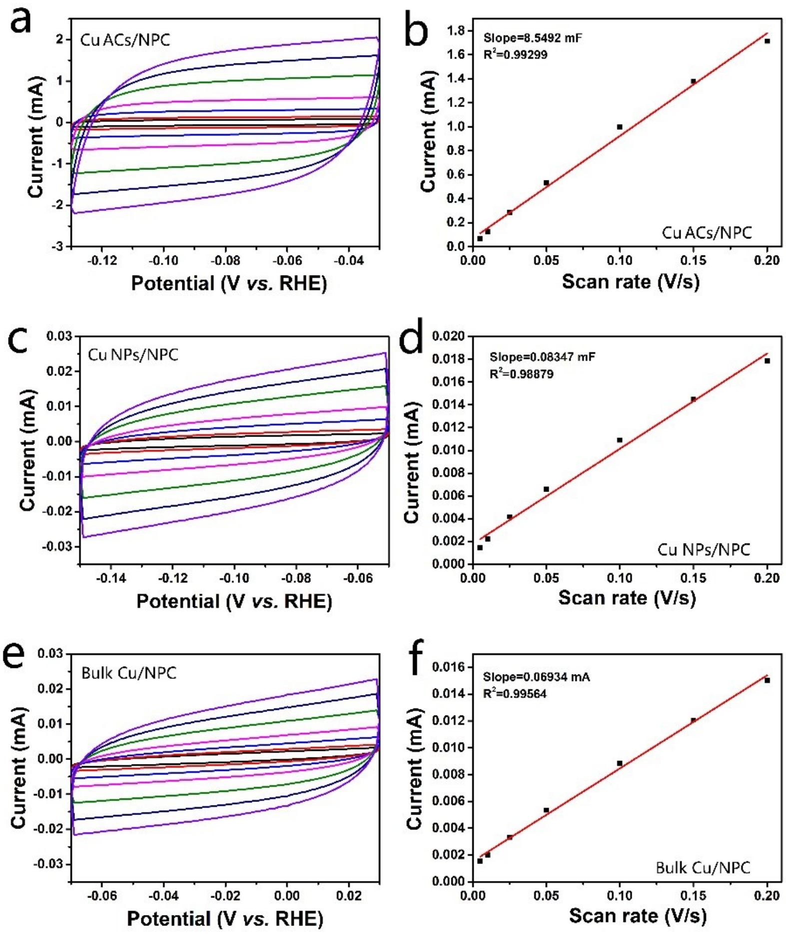

Figure S14. Double-layer capacitances of (a, b) Cu ACs/NPC, (c, d) Cu NPs/NPC and (e, f) Bulk Cu/NPC.

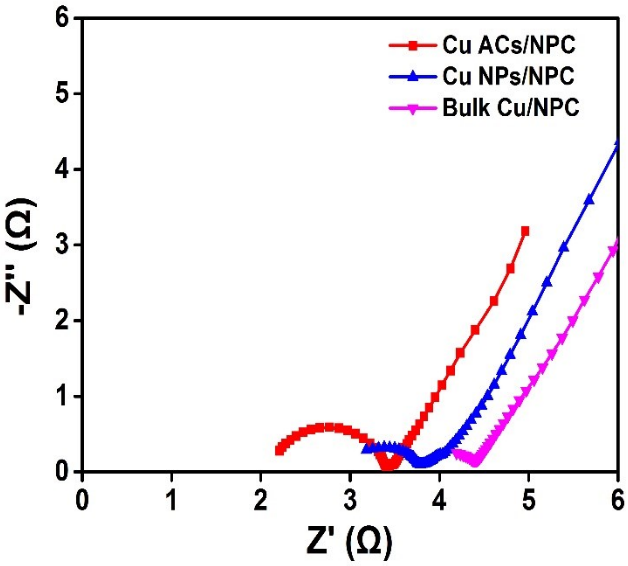

Figure S15. EIS Nyquist plots of Cu ACs/NPC (red line), Cu NPs/NPC (blue line) and Bulk Cu/NPC (pink line). The electrochemical impedance spectroscopy measurements were performed in 0.5 M $KHCO_3$ at -0.5 V (*vs.* RHE) with an amplitude of 5 mV of 1 to 10^5 Hz.

3. Supplementary Notes

3.1 Note 1

The mass specific partial current density was calculated by Supplementary equation[S3]:

$$j_{co} = \frac{I_{total} \times FE_{CO}}{m_{Cu}} \quad (3)$$

I_{total} is the total current at different potential; m_{Cu} is the Cu content of different samples quantified by ICP-MS.

3.2 Note 2

The electrochemically active surface area (ECSA) of all the electrocatalysts is estimated from the electrochemical double-layer capacitance (C_{dl}). In order to determine the C_{dl} values, the capacitive currents were tested in 5 M KOH solution *via* CV curves at different scan rates (0.005, 0.01, 0.025, 0.05, 0.1, 0.15 and 0.2 V s^{-1}) under a non-Faradaic potential range. The non-Faradaic potential range was identified from CV and the applied potential of CV was recorded within 0.1 V centered at the open-circuit potential. All measured currents in this region are assumed to be owing to a double-layer charging.

The electrochemical double layer capacitance C_{dl} can be calculated as follows:

$$C_{dl} = i_c/v \quad (4)$$

Where i_c is the charging current, and v is the scan rate.

The plot of i_c against v yields a straight line with a slope equal to C_{dl}.

The ECSA values of various samples were calculated from the double layer capacitance according to the following equation:

$$ECSA = C_{dl}/C_s \quad (5)$$

where C_s is the specific capacitance of the sample or the capacitance of an atomically smooth planar surface of the material per unit area under identical electrolyte conditions. As reported by previous reports, the specific capacitance of graphene materials is ~22 μF cm^{-2}.[S1,S2] Thus, the ECSA values for Cu ACs/NPC, Cu NPs/NPC and Bulk Cu/NPC were calculated to be 388.6 cm^2, 3.79 cm^2, and 3.15 cm^2, respectively.

3.3 Note 3

The $[HCO_3]^-$ dependence study was performed at a constant applied potential (-0.5 V *vs.* RHE) at the $KHCO_3$ concentrations varying from 0.5 to 0.1 M. KCl was added to the low $KHCO_3$ concentration solutions to maintain the same ionic strength.

3.4 Note 4

Turnover frequency (TOF) for CO_2RR was evaluated by Supplementary equation[S4]:

$$TOF = \frac{I_{product}/NF}{m_{cat} \times w/M_{Cu}} \times 3600\ (h^{-1}) \quad (6)$$

Where $I_{product}$ is the partial current for CO production; N is the number of electron exchanged, for instance, N=2 for the reduction of CO_2 to CO; F=96485.3 C/mol (Faraday constant); m_{cat} is the weight of catalyst loaded on the electrode; w is the Cu loading in the catalyst; M_{Cu} is the molar mass of Cu, 63.546 g/mol.[S3]

4. Supplementary Tables

Table S1. Cu contents in the samples obtained by ICP-MS.

Samples	Weight of samples (W: mg)	Metered volume (V_0: mL)	Concentration (C: ppb)	Dilution factor (I)	Content of Cu (wt.%)
Cu ACs/NPC	0.59	30	3.9785	10	0.2
Cu NPs/NPC	0.75	10	17.2520	100	2.3
Bulk Cu/NPC	0.75	10	35.9053	100	4.8

The content of Cu amount was calculated as follow:

$$Cu(wt\%) = \frac{C * V_0 * I * 10^{-6}}{W} \times 100 \quad (7)$$

Table S2. Structural parameters obtained from the EXAFS fitting results.

Sample	Path	CN	R (Å)	$\Delta\sigma^2$*(10^{-3} Å^2)
Cu ACs/NPC	Cu-O	3.9	1.94	6.35

CN is the coordination number; R is the interatomic distance; σ^2 is Debye-Waller factor.

Table S3. Comparison of the CO_2RR catalytic performance with Cu-based catalysts for CO production.

Catalyst	Potential (V *vs.* RHE)	Electrolyte	Products	FE (%)	J_{co} (mA cm^{-2})	Ref.
Cu ACs/NPC	-0.5	0.5 M $KHCO_3$	CO	93.21	5.09	This work
Cu-N_2/GN	-0.5	0.1 M $KHCO_3$	CO	81	1.701	S4
Cu-N_4/GN	-0.5	0.1 M $KHCO_3$	CO	62	0.744	S4
Cu-$N_{0.5}$NC	-0.6	0.1 M $CsHCO_3$	CO	75	2.5	S5
Cu-N_4-C	-0.74	0.1 M $KHCO_3$	CO	29	5.0	S6
Cu-Pd NP/C	-0.9	0.1 M $KHCO_3$	CO	87	47 mA mg_{Pd}^{-1}	S7
CuPolyPc@CNT	-0.7	0.1 M $CsHCO_3$	CO	80	7.5	S8
AgCu-50	-0.6	0.1 M $KHCO_3$	CO	58.4	-	S9
Cu Nanowires	-0.6	0.1 M $KHCO_3$	CO	~50	-	S10
Cu foam	-0.45	0.1 M $KHCO_3$	CO	~39	3.67	S11
Cu-N-C	-0.66	0.5 M $KHCO_3$	CO	21	1.68	S12

Table S4. Electrocatalytic characterization of Cu ACs/NPC, Cu NPs/NPC and Bulk Cu/NPC.

Sample	A_{ec} (cm_{ec}^2)	CO faradic efficiency (%)
Cu ACs/NPC	388.6	93.21
Cu NPs/NPC	3.79	5.09
Bulk Cu/NPC	3.15	1.27

J_{CO} is the CO partial current density calculated by multiplying the CO current efficiency by the measured current density (normalized by the electrode geometric area). A_{ec} is the electrochemical surface area measured by the double-layer capacitance method (Figure S14). The J_{CO} and CO current efficiency were measured at −0.5 V (*vs.* RHE).

Supplementary references:

S1 C. C. L. McCrory, S. Jung, J. C. Peters and T. F. Jaramillo, *J. Am. Chem. Soc.*, 2013, **135**, 16977–16987.

S2 S. Zhao, Z. Tang, S. Guo, M. Han, C. Zhu, Y. Zhou, L. Bai, J. Gao, H. Huang, Y. Li, Y. Liu and Z. Kang, *ACS Catal.*, 2018, **8**, 188–197.

S3 E. Zhang, T. Wang, K. Yu, J. Liu, W. Chen, A. Li, H. Rong, R. Lin, S. Ji, X. Zheng, Y. Wang, L. Zheng, C. Chen, D. Wang, J. Zhang and Y. Li, *J. Am. Chem. Soc.*, 2019, **141**, 16569–16573.

S4 W. Zheng, J. Yang, H. Chen, Y. Hou, Q. Wang, M. Gu, F. He, Y. Xia, Z. Xia, Z. Li, B. Yang, L. Lei, C. Yuan, Q. He, M. Qiu and X. Feng, *Adv. Funct. Mater.*, 2020, **30**, 1907658.

S5 D. Karapinar, N. T. Huan, N. Ranjbar Sahraie, J. Li, D. Wakerley, N. Touati, S.

Zanna, D. Taverna, L. H. Galvão Tizei, A. Zitolo, F. Jaouen, V. Mougel and M. Fontecave, *Angew. Chem. Int. Ed.*, 2019, **58**, 15098–15103.

S6 W. Ju, A. Bagger, G.-P. Hao, A. S. Varela, I. Sinev, V. Bon, B. Roldan Cuenya, S. Kaskel, J. Rossmeisl and P. Strasser, *Nat. Commun.*, 2017, **8**, 944.

S7 Y. Mun, S. Lee, A. Cho, S. Kim, J. W. Han and J. Lee, *Appl. Catal. B Environ.*, 2019, **246**, 82–88.

S8 D. Karapinar, A. Zitolo, T. N. Huan, S. Zanna, D. Taverna, L. H. Galvão Tizei, D. Giaume, P. Marcus, V. Mougel and M. Fontecave, *ChemSusChem*, 2020, **13**, 173–179.

S9 T. Kottakkat, K. Klingan, S. Jiang, Z. P. Jovanov, V. H. Davies, G. A. M. El-Nagar, H. Dau and C. Roth, *ACS Appl. Mater. Interfaces*, 2019, **11**, 14734–14744.

S10 M. Ma, K. Djanashvili and W. A. Smith, *Phys. Chem. Chem. Phys.*, 2015, **17**, 20861–20867.

S11 S. Min, X. Yang, A.-Y. Lu, C.-C. Tseng, M. N. Hedhili, L.-J. Li and K.-W. Huang, *Nano Energy*, 2016, **27**, 121–129.

S12 A. Roy, D. Hursán, K. Artyushkova, P. Atanassov, C. Janáky and A. Serov, *Appl. Catal. B Environ.*, 2018, **232**, 512–520.